Agricultural and Forest Meteorology 356 (2024) 110150

Contents lists available at ScienceDirect

Agricultural and Forest Meteorology

journal homepage: www.elsevier.com/locate/agrformet

Ozone dose-response relationships for wheat can be derived using photosynthetic-based stomatal conductance models

P. Pande [a,*], F. Hayes [b], S. Bland [a], N. Booth [c], H. Pleijel [d], L.D. Emberson [c]

[a] Stockholm Environment Institute at York, Environment & Geography Dept., University of York, YO10 5DD, United Kingdom
[b] UK Centre for Ecology & Hydrology, Environment Centre Wales, Deiniol Road, Gwynedd, Bangor, LL57 2UW, United Kingdom
[c] Environment & Geography Dept., University of York, YO10 5DD, United Kingdom
[d] Department of Biological and Environmental Sciences, University of Gothenburg, Box 461, 40530 Gothenburg, Sweden

ARTICLE INFO

Keywords:
Phytotoxic ozone dose
Grain yield
Photosynthesis
Crop modelling
Flux-response relationship

ABSTRACT

Ground-level ozone (O_3) pollution occurs across many important agricultural regions in Europe, North America, and Asia, negatively impacting O_3-sensitive crops such as wheat. Risk assessment methods to quantify the magnitude and spatial extent of O_3 pollution have often used dose-response relationships. In Europe, the dose metrics used in these relationships have evolved from concentration- to flux-based metrics since stomatal O_3 flux has been found to correlate better with yield losses. Estimates of stomatal conductance (g_{sto}) have to date used an empirical multiplicative model. However, other more mechanistic approaches are available, namely the coupled photosynthetic-stomatal conductance ($A_{net}g_{sto}$) model. This study used a European O_3 OTC and solardome fumigation experimental dataset (comprising 6 cultivars, 4 countries and 14 years) to develop a new flux-based dose-response relationship for wheat yield using the mechanistic $A_{net}g_{sto}$ model ($A_{net}g_{sto}mech$). The $A_{net}g_{sto}mech$ model marginally improved the regression of the dose-response relationship ($R^2 = 0.74$) when compared to the flux-response models derived from empirical g_{sto} models. In addition, the $A_{net}g_{sto}mech$ model was somewhat better at predicting the effect of high O_3 concentrations on diurnal and seasonal profiles of g_{sto} and A_{net}. It was also better able to simulate changes of up to 7 and 12 days, respectively, in the start (SOS) and end (EOS) of senescence, an important determinant of yield loss, over a range of O_3 treatments. We conclude that $A_{net}g_{sto}mech$ model can be used to derive robust flux-response relationships.

1. Introduction

Empirical evidence from Europe, North America and Asia shows that O_3 is causing a range of impacts on staple crops such as wheat (Hansen et al., 2019; Feng et al., 2022; Büker et al., 2015). These impacts include altered stomatal conductance (g_{sto}) (Danielsson et al., 2003; Ghosh et al., 2020), reduced photosynthesis (A_{net}) (Ojanperä et al., 1998) and early and enhanced leaf senescence (Osborne et al., 2019; Gelang et al., 2000). Effects on leaf senescence can lead to a reduction in A_{net} and g_{sto} and a shorter grain-filling period (Gelang et al., 2000) thus decreasing yield (Pleijel et al., 2022) and biomass (Feng et al., 2021). Experimental meta-analyses have found that wheat yield losses can range from 3 to 50 % when O_3 concentrations (described as a 7hr daylight mean over the growing season) range from 5 to 115 ppb (Mills et al., 2018). Risk assessments performed on application of dose-response relationships derived from such experimental data (Pleijel et al., 2007) estimate O_3 induced yield losses of between 12 and 15 % globally, causing production losses of approximately 85 million tonnes (Mills et al., 2018). These losses in productivity are a cause for concern, given the importance of wheat as a staple crop for approximately 35 % of the global population (Grote et al., 2021) and that the annual consumption of wheat worldwide is approximately 791 million tonnes (United States Department of Agriculture, 2023). Evidence also suggests that the threat from O_3 pollution will continue into the future. Background O_3 concentrations have remained high over agriculturally important regions (Feng et al., 2019; Arnold et al., 2021; Boleti et al., 2020; Sicard et al., 2021) across Europe (Rega et al., 2020) and both background and peak O_3 concentrations are increasing in the Indo-Gangetic plains in south Asia (Shah et al., 2019), and the North China Plain in East Asia (Liu et al., 2016). To estimate the threat from O_3 pollution, risk assessment modelling methods have been developed to assess the current and future effects of O_3 on crop growth and yield at national, regional, and global scales

* Corresponding author.
E-mail address: pritha.pande@york.ac.uk (P. Pande).

https://doi.org/10.1016/j.agrformet.2024.110150
Received 23 August 2023; Received in revised form 3 May 2024; Accepted 2 July 2024
Available online 23 July 2024

(Emberson et al., 2018). These methods often use experimental O_3 filtration/fumigation data to derive dose-response relationships and hence require the identification of a suitable dose metric capable of predicting O_3 damage (i.e., yield loss for crops). Metrics would ideally be able to incorporate the effects of species and cultivar as well as management practices (e.g. irrigation) that are known to alter sensitivity to O_3 pollution (Mills et al., 2018; Anav et al., 2016; Osborne et al., 2019). Metrics have evolved over the past decade moving from concentration- to flux-based indices (Grulke and Heath, 2019; Pleijel et al., 2007; Mills et al., 2018) with the flux-based approach allowing O_3 concentrations to be decoupled from O_3 exposure when conditions (e.g., high atmospheric or soil water deficits) limit stomatal O_3 uptake (Emberson et al., 2018; Tai et al., 2021). This capability of the flux-based approach has been shown to give more reliable estimates of the spatial extent of O_3 damage (Mills et al., 2011).

Consequently, the stomatal O_3 flux metric, denoted as Phytotoxic Ozone Dose (PODy) has been adopted by the UNECE Convention on Long-Range Transboundary Air Pollution (LRTAP) to develop dose-response relationships for the derivation of 'critical levels' for Europe; these are levels below which crop damage would not be expected to occur according to current knowledge (LRTAP Convention, 2017). These 'critical levels' have been used to establish national and regional air quality standards for the formulation of emission reduction policy (Massman et al., 2000; Emberson et al., 2000; Mills et al., 2011). Current flux-response relationships have been developed using an empirical multiplicative g_{sto} model (LRTAP Convention, 2017), a component of the DO$_3$SE O_3 deposition model used in European scale modelling (Simpson et al., 2012) to calculate stomatal O_3 flux for crops grown in European filtration/fumigation experiments. This approach allows accumulated stomatal O_3 flux (PODy) to be calculated over a growing season and plotted against relative yield loss for a range of experimental O_3 treatments. A response relationship can then be derived from statistical linear regression of these pooled data points (Pleijel et al., 2022). In Europe, flux-response relationships for wheat are based on data from 4 European countries, encompassing 14 years and 6 cultivars (LRTAP Convention, 2017).

An important criticism and limitation of existing flux-response relationships is that the estimate of g_{sto} is not related to the plant's main physiological requirement for gas exchange, which is the uptake of CO_2 for carbon assimilation by photosynthesis. This creates a disconnect between O_3 stomatal uptake and critical physiological processes such as photosynthesis, respiration, carbon accumulation, and allocation, development, growth, and yield (Ball et al., 1987; Wang et al., 2009). Stomatal conductance models coupled to photosynthesis were developed in the early 1990s (Leuning et.al., 1995) and work on a supply and demand basis whereby stomatal opening regulates the CO_2 availability (supply) and the photosynthetic process in the leaf's chloroplasts determines the plant's need for CO_2 (demand), thereby controlling g_{sto} according to the requirements for photosynthesis. These models are more complex than the empirical multiplicative g_{sto} model since they require an estimate of photosynthesis, which often involves applying a biochemical model to simulate plant physiological processes (Büker et al., 2007; Op De Beeck et al., 2010). However, using a multiplicative model requires more parameters and cannot consider the interaction of different environmental variables at the same time. Using an $A_{net}g_{sto}$ approach would also allow a more mechanistic representation of O_3 effects on growth and yield to be explored (Emberson et al., 2018; Büker et al., 2007). This is important as O_3 is thought to cause damage *via* both an instantaneous effect on photosynthesis as well as a longer-term effect that induces early onset senescence which may lead to earlier maturity and a shorter time period for grain filling (Ewert and Porter, 2000; Emberson et al., 2018).

In this paper, we develop leaf level $A_{net}g_{sto}$ models suitable for quantifying stomatal O_3 flux. The aims of this paper are (i) to assess the ability of the multiplicative g_{sto} and $A_{net}g_{sto}$ models (an empirical $A_{net}g_{sto}$ model ($A_{net}g_{sto}emp$) and a mechanistic $A_{net}g_{sto}$ model ($A_{net}g_{sto}mech$)) to simulate g_{sto} (and A_{net}), (ii) to assess the ability of $A_{net}g_{sto}$ models to simulate O_3 damage to photosynthesis and leaf senescence, and (iii) to compare the ability of multiplicative g_{sto} and $A_{net}g_{sto}$ models to simulate yield loss and hence derive flux-response relationships. This will be achieved by re-analysis of the European wheat flux-response data used to derive the current UNECE LRTAP Convention flux response relationship (LRTAP Convention, 2017) along with additional data from the UK and Sweden which provide further insight into the effects of O_3 concentrations on leaf physiology and senescence. These three models were not designed to simulate dynamic crop growth or yield but rather to estimate cumulative stomatal O_3 flux for regression against yield to develop flux response relationships. The models can be tested against observed A_{net}, g_{sto} and Chlorophyll Content Index (CCI) data to assess their ability in simulating key aspects of leaf physiology that determine O_3 uptake and damage.

2. Methods

2.1. Stomatal conductance models

2.1.1. $g_{sto}emp$ model

The $g_{sto}emp$ model is an empirical model that estimates g_{sto} according to environmental modifications to a species-specific maximum stomatal conductance value (g_{max}) (Jarvis, 1976; Emberson et al., 2000; Pleijel et al., 2007) written as;

$$g_{sto} = g_{\max}.\left[\min\left(leaf\ f_{phen},\ f_{O3}\right).f_{light}.\max\left\{f_{\min},\ \left(f_{temp}.f_{VPD}.f_{SWP}\right)\right\}\right] \quad (1)$$

Where g_{sto} is the flag leaf stomatal conductance (mmol O_3 m^{-2} PLA s^{-1} where PLA is the projected leaf area) and g_{max} is the species-specific maximum g_{sto}. The parameters *leaf* f_{phen}, f_{O3}, f_{light}, f_{temp}, f_{VPD}, and f_{SWP} account for the effect of phenology, O_3, light, temperature, vapour pressure deficit (VPD), and soil water potential (SWP) on g_{max}. f_{min} is the fractional minimal daylight g_{sto}. These functions have values ranging from 0 to 1. Since wheat grown in the filtration/fumigation studies was always well-watered, we assume that f_{SWP} equals 1. The DO$_3$SE algorithms and parameters for these functions are described in equations S1-S5 and Table S1 respectively after Grünhage et al. (2012) and the LRTAP Convention (2017).

2.1.2. $A_{net}g_{sto}emp$ model

The coupled $A_{net}g_{sto}emp$ model provides a consistent estimate of the exchange of CO_2 (driven by supply and demand of CO_2 for photosynthesis and its products) on consideration of water loss controlled by g_{sto}. The $A_{net}g_{sto}emp$ model consists of a combination of two separate models: a) the mechanistic and biochemical photosynthesis model (Farquhar et al., 1980; Harley et al., 1992) that estimates net photosynthesis (A_{net}), and b) the coupled $A_{net-}g_{sto}$ model of (Leuning, 1995) that estimates g_{sto}.

The A_{net} model assumes that photosynthesis is limited, according to prevailing environmental conditions, by three different mechanisms: i. rubisco activity (A_c); ii. the regeneration of ribulose-1,5-bisphosphate (RuBP) which is limited by the rate of electron transport (A_j) and iii. the rate of transport of photosynthetic products (A_p) (Sharkey et al., 2007). These influences on A_{net} are calculated by determination of the smaller of these theoretical CO_2 assimilation rates less the rate of dark respiration (R_d) (Harley et al., 1992), see equations [2] to [5].

$$A_{net} = \min(A_c, A_j,\ A_p) - R_d \quad (2)$$

where;

$$A_c = \frac{(C_i - \Gamma^*).Vc_{max25}.f_{O3}.\ leaf\ f_{phen}}{C_i + K_c\left(1 + \frac{O_i}{K_o}\right)} \quad (3)$$

$$A_j = J.\frac{C_i - \Gamma*}{a.C_i + b.\Gamma*} \tag{4}$$

$$A_p = 0.5 \ . \ V_{cmax25} \tag{5}$$

Where V_{cmax25} is the maximum rate of RuBP carboxylation catalysed by the enzyme Rubisco at 25 °C (leaf temperature), C_i and O_i are the intercellular CO_2 and O_2 concentrations respectively; K_c and K_o are the Rubisco Michaelis-Menten constants for CO_2 and O_2 respectively; $\Gamma*$ is the CO_2 compensation point in the absence of respiration. J is the electron transport rate, which increases linearly with incident photosynthetically active photon flux density (Q, μmol/m^2/s) until light saturation is reached, beyond which J approaches a maximum value known as J_{max} (Buker et.al., 2007). c_s is the CO_2 concentration at the leaf surface and Γ is the CO_2 compensation point, calculated according to Buker et al. (2007).

In the photosynthetic model by Sharkey et al. (2007), the parameters 'a' and 'b' reflect conservative estimates for the electron transport rate during carboxylation and oxygenation, assumed to be 4 and 8 electrons respectively, allowing for the regeneration of RuBP and the formation of NADPH and ATP in the Calvin cycle. A_c is modified to include f_{O3} and *leaf* f_{phen} to empirically define the effect of leaf age and O_3 induced senescence on g_{sto} (Ewert et al., 1999). This allows V_{cmax25} to change throughout the growing season. Since O_3 primarily causes a limitation to Rubisco (Ewert et al., 1999), we do not include O_3 damage in estimates of A_j and A_p.

g_{sto} is calculated from A_{net} using an empirical relationship between g_{sto}, A_{net} and environmental variables following an approach first developed by Ball et al. (1987) and modified by Leuning (1995) as described in equation [6].

$$g_{sto} = \left[g_{min} + \left(m.A_{net}.f_{VPD}\right) / \left(c_s - \Gamma\right)\right] \tag{6}$$

Where g_{min} is the minimal daylight g_{sto} value (Leuning,1995). The parameter m describes the species-specific sensitivity to A_{net} and CO_2 concentration at the leaf surface. c_s is the CO_2 concentration at the leaf surface and Γ is the CO_2 compensation point calculated according to Buker et al. (2007).

The use of the multiplicative g_{sto} models f_{VPD} relationship (Danielsson et al., 2003; Pleijel et al., 2007; LRTAP Convention, 2017) ensures consistency between the $g_{sto}emp$ and $A_{net}g_{sto}emp$ modelling methods used in this study, see equation [7].

$$f_{VPD} = \left(1 + \left(\frac{VPD}{VPDo}\right)^8\right)^{-1} \tag{7}$$

where $VPDo$ is the VPD threshold (Leuning et al.,1998) parameterised to reflect a more gradual decrease in g_{sto} with increasing VPD compared to that previously suggested by Leuning's (1995) hyperbolic function (see Fig S1). The $A_{net}g_{sto}emp$ model follows the same method as used in the $g_{sto}emp$ model to calculate the O_3 (i.e. the f_{O3} function) and phenology (i.e. the *leaf* f_{phen} function) effect on conducatance. The only structural difference between the $A_{net}g_{sto}emp$ and $A_{net}g_{sto}mech$ model lies in a more mechanistic approach in the latter to model these effects..

2.1.3. $A_{net}g_{sto}mech$ model

The $A_{net}g_{sto}mech$ model simulates the loss of instantaneous photosynthetic activity and the acceleration of leaf senescence using a mechanistic approach to modify the Rubisco-limited rate of photosynthesis (A_c) following the approach of Ewert & Porter (2000) as described in equation [8].

$$A_c = \frac{(C_i - \Gamma^*).Vc_{max}.fO_{3,s}(d).\ f_{LS}}{C_i + K_c\left(1 + \frac{O_i}{K_o}\right)} \tag{8}$$

The short-term impact of O_3 on A_c is calculated according to the $fO_{3,s}(d)$ term, the cumulative daylight hour effect of O_3 on Vc_{max}, which allows for an instantaneous effect of O_3 on photosynthesis when stomatal O_3 flux overwhelms detoxification and repair mechanisms (Betzelberger et al., 2012; Feng et al., 2022). $fO_{3,s}(d)$ is estimated by calculating $f_{O3,s}(h)$ (representing the linear relationship between stomatal O_3 flux (f_{st})) and a decrease in A_c calculated for every hour as described in equation [9]

$$\begin{aligned} f_{O3,s}(h) &= 1;\ for\ f_{st} \le \frac{\gamma1}{\gamma2} \\ f_{O3,s}(h) &= 1 + \gamma1 - \gamma2 * f_{st};\ for \frac{\gamma1}{\gamma2} < f_{st} < \frac{1+\gamma1}{\gamma2} \\ f_{O3,s}(h) &= 0;\ for\ f_{st} \ge \frac{1+\gamma1}{\gamma2} \end{aligned} \tag{9}$$

where $\gamma1$ and $\gamma2$ are both short-term O_3 damage coefficients, with $\frac{\gamma1}{\gamma2}$ representing the O_3 detoxification threshold below which no damage occurs to the photosynthetic system and $\gamma2$ determines the effect of f_{st} on A_c, see Section 2.2 for the f_{st} calculation, which is estimated for the previous hour. $fO_{3,s}(d)$ and $f_{O3,s}(d-1)$ are calculated as described in equation [10].

$$\begin{aligned} f_{O3,s}(d) &= f_{O3,s}(h) * r_{O3,s};\ for\ PAR \le 50\ W\ m^{-2} \\ f_{O3,s}(d) &= f_{O3,s}(h) * f_{O3,s}(d-1);\ for\ PAR > 50\ W\ m^{-2} \end{aligned} \tag{10}$$

Where the term $f_{O3,s}(d)$ describes the instantaneous O_3 effect on Vc_{max25} which is allowed to build over the course of the daylight period (when photosynthetically active radiation (PAR) is greater than 50 W m^{-2}) from an initial value which is determined by the previous days $f_{O3,s}(d-1)$ value and an allowance for incomplete overnight recovery in Vc_{max25} which varies with leaf age as described by $r_{O3,s}$ term in equation [11].

$$r_{O3,s} = f_{O3,s}(d-1) + \left(1 - f_{O3,s}(d-1)\right) * f_{LA} \tag{11}$$

Where f_{LA} defines leaf age and is calculated as

$$\begin{aligned} f_{LA} &= 1; for\ TT_{leaf} \le tl, em \\ f_{LA} &= 1 - \frac{(tl - tl_{em})}{tl_{ma}}; for\ tl, em < TT_{leaf} < tl \\ f_{LA} &= 0; for\ TT_{leaf} \ge tl \end{aligned} \tag{12}$$

The long-term impact of O_3 on Vc_{max25} represented by the f_{Ls} term represents the longer-term accumulation of stomatal O_3 flux (acc_{fst}) causing degradation to the Rubisco enzyme triggering early and enhanced senescence of mature leaves (Gelang et al., 2000; Osborne et al., 2019). The simulation of f_{Ls} (and f_{LA} used in the short-term O_3 effect) are related to thermal time defined periods over the course of the flag leaf life span defined as a mature (tl, ep) and a senescing (tl, se) stage which together comprise the full flag leaf lifespan (tl, ma), equivalent to *leaf* f_{phen} in the empirical models. The tl, ep stage defines the period between the start of anthesis and start of senescence (SOS). The tl, se stage simulates the decline in chlorophyll content and depicts the period between SOS and the end of senescence (EOS), see Section 2.4 for the SOS and EOS calculation. TT_{leaf} represents the cumulative thermal time. This value is determined by integrating daily mean temperature over a 24-hour period and accumulating over the course of the growing season.

Equations S5 and S6 give the *leaf* f_{phen} and tl, ma equations and Fig. S2 describes the relationship between *leaf* f_{phen}, f_{LS} and f_{LA}. The O_3 effect on f_{Ls} is first simulated by estimating a weighted accumulated fst ($fO3, l$) modified from Ewert and Porter (2000) by

$$fO3_l = 1 - \max\left(\min\left(\gamma3 * POD_y, 1\right), 0\right) \tag{13}$$

where $\gamma3$ determines the reduction in tl, ma as POD_y (in μmol m^{-2}) increases and POD_y is calculated as described in equation [19].

The SOS is determined by $\gamma4$, whilst $\gamma5$ determines maturity (or EOS).

$$\begin{aligned} tl_{ep_{O3}} &= tl_{ep} * (1-((1-fO3_l)*\gamma 4)) \\ tl_{se_{O3}} &= tl_{se} * (1-((1-fO3_l)*\gamma 5)) + zc \end{aligned} \quad (14)$$

$$zc = tl_{ep} - tl_{ep_{O3}} \quad (15)$$

Where, $tl_{ep_{O3}}$ is tl_{ep} with an O_3 effect which may bring the onset of senescence earlier, and $tl_{se_{O3}}$ is $tl_{se}$with an O_3 effect which may bring maturity earlier. f_{Ls} is estimated by,

$$\begin{aligned} f_{Ls} &= 1; for\ TT_{leaf} \leq tl, em + tl, ep \\ f_{Ls} &= 1 - \frac{TT_{leaf} - tl_{em} - tl_{ep_{O3}}}{tl_{se_{O3}}}; for\ tl, em + tl, ep < TT_{leaf} < tl \\ f_{Ls} &= 0;\ \ for\ TT_{leaf} \geq tl \end{aligned} \quad (16)$$

2.2. Estimation of O_3 uptake (f_{st}) and PODy

For all models used in this study f_{st} (in nmol O_3 PLA m^{-2} s^{-1}) is calculated as a function of O_3 concentration at the leaf boundary layer, g_{sto} and O_3 deposition to the external leaf surface (see equations [17], [18] and [19]) following the LRTAP Convention (2017).

$$f_{st} = [O3] * (gsto) * \left(\frac{leaf_{rc}}{(leaf_{rb} + leaf_{rc})}\right) \quad (17)$$

$$leaf_{rb} = 1.3 * 150 * sqrt\left(\frac{Lm}{uh}\right) \quad (18)$$

$$leaf_{rc} = \frac{1}{(gsto + gsto_{ext})} \quad (19)$$

Where $[O3]$ is the O_3 concentration at the upper surface of the quasi-laminar boundary layer of the flag leaf (nmol/mol); *gsto* is leaf stomatal conductance (m/s) as described in Eqn 1 and 6, $leaf_{rb}$ is the quasi laminar leaf boundary layer resistance (s/m), *Lm* is the cross wind leaf dimension (m), *uh* is the windspeed at the canopy surface (m/s), $leaf_{rc}$ is leaf surface resistance (s/m), and *gext* is the external plant cuticle conductance (m/s). Here we assume that the O_3 concentrations measured within the field chambers of the filtration/fumigation experiments represent a reasonable estimate of O_3 at the leaf boundary layer due to the enhanced air circulation. Parameter values are provided in Table S3.

This study uses the *PODy* stomatal flux-based index currently used by the LRTAP Convention (2017) to assess damage to European wheat calculated using a *y* threshold value of 6 nmol O_3 m^{-2} PLA s^{-1} according to equation [20] for all three models.

$$POD_y = \sum_{i=1}^{n} [f_{sti} - y] * \left(\frac{3600}{10^6}\right);\ for\ f_{sti} \geq y\ nmol\ m^2\ PLA\ s^{-1} \quad (20)$$

where f_{sti} is the hourly mean O_3 flux in nmol O_3 m^{-2} PLA s^{-1} (see equation [17]) and *n* is the number of hours within the accumulation period. *y* (equivalent to $\frac{\gamma 1}{\gamma 2}$) is equal to 6 (nmol m^{-2} PLA s^{-1}) and is subtracted from each hourly averaged f_{st} (nmol O_3 m^{-2} PLA s^{-1}) value only when $f_{st} > y$, during daylight hours (i.e. when PAR > 50 W m^{-2}). The term ($3600/10^6$) converts to hourly fluxes and to mmol O_3 m^{-2} PLA. This method estimates *POD*6 on a per m^2 basis representative of the flag leaf only; it takes no account of the actual LAI of the flag leaf (or other canopy leaves), that might be contributing to carbon assimilate and hence influence O_3 damage. This assumption may warrant further investigation were canopy O_3 uptake considered an important determinant of ozone damage. However, at least for wheat, the importance of the flag leaf in providing carbon assimilate for grain filling likely makes this a reasonable assumption.

2.3. Datasets

The g_{sto} models were applied to simulate POD_6 for O_3 filtration/fumigation experimental datasets conducted since the 1980s in Europe that described wheat yield losses due to different O_3 treatments. These datasets represent 4 countries (Belgium, Sweden, Finland, and United Kingdom) 6 cultivars and 14 years. These are predominantly the same data used to derive the UNECE LRTAP flux-response relationships (LRTAP Convention, 2017) (exceptions being the exclusion of an Italian dataset which used a variety of *Durum* wheat), and the inclusion of new data from the UK and Sweden which have the benefit of also providing important physiological and chlorophyll content data. A detailed description of these datasets is given in the Table S2.

2.4. Parameterisation for the g_{sto} models

The multiplicative g_{sto} model uses the same parameters as described in the LRTAP Convention (2017). Full details are provided in Table S1.

Both the $A_{net}g_{sto}emp$ *and* $A_{net}g_{sto}mech$ models require parameterisation of V_{cmax25}, J_{max25} and *m*. Parameters, such as g_{min}, representing the minimum stomatal conductance (set to 0.01 μmol CO_2 m^{-2} s^{-1}), are sourced from (Ewert and Porter, 2000), while VPD_0 (set at 2.2 kPa and detailed in Section 2.2) are determined empirically.

However, the $A_{net}g_{sto}mech$ model requires additional parameterisation for the O_3 damage module (represented by γ coefficients). By contrast, the $A_{net}g_{sto}emp$ model uses the same fO_3 function as the multiplicative g_{sto} model for estimating O_3 damage and therefore does not need additional calibration.

A systematic literature review was conducted to extract data to define the likely range and initial values (range mean) of V_{cmax25}, J_{max25} and *m* values occurring in wheat across Europe (see section SF); this approach is similar to that used to parameterise the $g_{sto}emp$ model (LRTAP Convention, 2017). V_{cmax25} and J_{max25} values were recorded for fully developed flag leaves growing under ambient atmospheric concentrations of O_3 and CO_2 for crops grown in the field/or large pots under a stress-free environment (see Fig. S3). Information describing the bio-geographic region and the prevalence of rainfed or irrigated management were also recorded (Fig. S4). A diagrammatic representation of the systematic literature review is provided in Fig. S5.

The parameterisation of *m* needs to be considered in relation to VPD_0 since the slope of the relationship *m* found when plotting A_{net} against g_{sto} represents a compromise between the cost and benefit of g_{sto} relative to CO_2 uptake for photosynthesis *vs* water loss affecting intrinsic water use efficiency (Medlyn et al., 2011). Here we follow the approach of Medlyn et al. (2011) and calibrate *m* to ensure that the modelled maximum A_{net} against g_{sto} aligns with the maximum observed A_{net} against g_{sto} values.

The parameters $\gamma 3$, $\gamma 4$, and $\gamma 5$ are only used in the $A_{net}g_{sto}mech$ damage module to simulate the rate of senescence. They were calibrated to ensure that the start (SOS) and end (EOS) of the senescence period matched observed senescence timings. These observations were derived from data describing the Chlorophyll Content Index (CCI) using the 'break point' analysis method (Mariën et al., 2019). This method determines the change in the seasonal pattern of CCI (and hence senescence) as a function of day of the year through piecewise linear regressions. The first segment of the regression (i.e. leaf expansion to mid-anthesis) was constrained to zero since it is assumed the leaf does not undergo senescence during this period. The slope of the second segment (from mid-anthesis to harvest) was allowed to be greater than zero on the assumption that senescence of the flag leaf will only occur after mid-anthesis. The slope with the lowest RMSE, indicating the smallest deviation between the measured CCI data points and the values estimated by the piecewise linear regression model, was assumed as the breakpoint for the SOS. Furthermore, a polynomial regression line, which delineates the period of senescence, was employed to determine EOS. The SOS and EOS of the flag leaf determined from break-point analysis of the UK (2015) and Swedish (1997 and 1999) datasets are given in the Table S4.

Details of the initial values and associated ranges for calibration of all $A_{net}g_{sto}$ parameters are provided in Table 1.

2.5. Calibration of the $A_{net}g_{sto}emp$ and $A_{net}g_{sto}mech$ models

The parameters for the $g_{sto}emp$ model were taken directly from LRTAP Convention (2017) and as such further calibration adjustments were not performed in this study.

The $A_{net}g_{sto}mech$ and $A_{net}g_{sto}emp$ model calibration for European conditions is performed in steps (as outlined below) using g_{sto}, *A_{net} and CCI data* from various sub-sets of the fumigation/filtration dataset. Fig. 1 presents a schematic diagram of the calibration process used for the $A_{net}g_{sto}$ models.

In the first step, initial values for V_{cmax25}, J_{max25} and m are selected that give a maximum g_{sto} value of between 500 and 600 mmol O_3 m^{-2} PLA s^{-1} and a maximum A_{net} value of between 30 and 35 µmol CO_2 m^{-2} s^{-1}. These values are consistent with the experimental dataset for Bangor as well as published studies that provide values for these parameters across Europe (Uddling and Pleijel, 2006; Sharma et al., 2015). This step only uses the low O_3 treatment data from Bangor ($n = 14$, see section SH) to ensure leaf physiology is unaffected by O_3.

In the second step, which is only performed for the $A_{net}g_{sto}mech$ model, the focus is on establishing initial values for O_3 damage parameters ($\gamma1$ to $\gamma5$) using datasets from both low ($n = 11$) and very high ($n = 10$) O_3 treatments from Bangor (see section SH). The O_3 coefficients $\gamma1$ and $\gamma2$ were set to give a detoxification threshold of 6 nmol O_3 $m^{-2}s^{-1}$, while $\gamma3$, $\gamma4$, $\gamma5$ were calibrated based on the observed SOS and EOS data, identified using the breakpoint method discussed in Section 6. O_3 damage parameters for the $A_{net}g_{sto}emp$ model are used as provided in the LRTAP Convention (2017) based on the f_{O3} function (and so consistent with the methods used in the $g_{sto}emp$ model).

Moving to the third step, model calibration uses all O_3 treatment data, segmenting these data into training and test sets as detailed in the Table S5. This uses a bootstrapping resampling technique (Hesterberg, 2011), using R software 4.2.3, to create bootstrap samples ($n = 5$) that randomly select a dataset with replacement i.e., in a sample, there can be duplicates of the same dataset (Table S5). Such an approach ensures that the initial parameters from steps one and two, along with their defined ranges drawn from both these steps and existing literature, are robustly tested across diverse data combinations from the fumigation/filtration experiments.

The calibration process then proceeds with these training samples ($n = 5$), aiming to calibrate the model to find the best parameters for V_{cmax25}, J_{max25} and m, and O_3 damage parameters ($\gamma3$ to $\gamma5$, only for the $A_{net}g_{sto}mech$ model). This calibration employs a computational genetic algorithm (Wang, 1997), an optimisation technique, with gradient descent to find the best parameters. The process requires an initial value and a range, and uses a combination of crossover strategy (selecting parameters randomly from parameter pairings) and mutation strategy (which takes a parameter range and uses incremental step changes) to identify the parameters with the highest R^2 and lowest RMSE value. Finally, the calibration outcomes from each training sample are aggregated, using weighted averages following Eq. S7, to establish the final

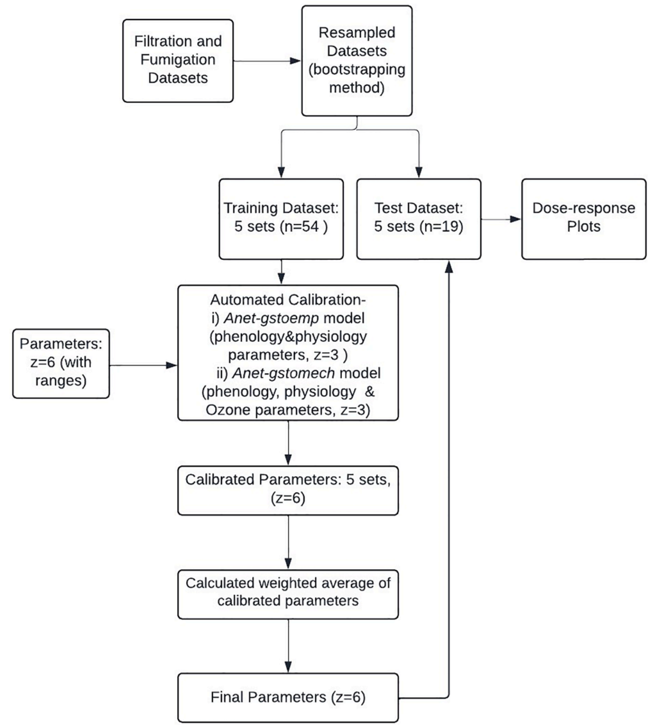

Fig. 1. Schematic diagram of the calibration process used for the $A_{net}g_{sto}$ models. This describes the number of filtration/fumigation datasets used for both the training and testing of model performance in relation to the automated calibration of various parameters dependent upon the construct of the $A_{net}g_{sto}emp$ and $A_{net}g_{sto}mech$ models. 'n' and 'z' refer to the number of datasets and parameters used, respectively.

Table 1
A detailed overview of the parameters, ranges, and optimised values after calibration of the $A_{net}g_{sto}$ models.

Parameters	Description	Units	Initial Parameter	Range	Parameters used (This study)	Reference
V_{cmax25}	Maximum catalytic rate at 25 °C	µmol CO_2 m^{-2} s^{-1}	90	60–180	88.91	(Büker et al., 2007) systematic literature review (this study)
J_{max25}	Maximum rate of electron transport at 25 °C	µmol CO_2 m^{-2} s^{-1}	180	150–250	173.83	
m	Species-specific sensitivity to A_{net}	–	7	5–15	7.87	(Kosugi et al., 2003; Collatz et al., 1991; Baldocchi and Meyers, 1998; Miner,Bauerle and Baldocchi, 2017)
$\gamma1$ *	Short term O_3 impact coefficient		0.027	–	0.027	(Ewert and Porter, 2000)
$\gamma2$ *	Short term O_3 impact coefficient	(nmol O_3 m^{-2} s^{-1})$^{-1}$	0.0045	–	0.0045	
$\gamma3$ *	Long term O_3 impact coefficient	(µmol O_3 m^{-2})$^{-1}$	0.1	0.1–0.7	0.11	Break point method (this study, see section 6)
$\gamma4$ *	Long term O_3 impact coefficient		0.1	0.1–0.5	0.16	
$\gamma5$ *	Long term O_3 impact coefficient		0.1	0.1–0.5	0.44	

*γ parameters only used for $A_{net}g_{sto} + O_{3\ mech}$.

set of parameters. These parameters are then used to run the models to estimate POD_6 and hence construct the flux-response relationships (Fig. S7), ensuring the model's applicability and accuracy.

The model's efficacy is then tested using test datasets ($n = 5$), which apply these final parameters. The performance metrics for these tests, specifically the R^2 and RMSE values for the flux-response relationships, give an indication of the model's reliability and precision across different datasets.

3. Results

3.1. Leaf physiology

Leaf physiology data (g_{sto} and A_{net}) from the UK were used to assess the ability of the different models to simulate key physiological variables necessary to estimate POD_y under both low background and peak O_3 treatments over the course of the growing season.

Fig. 2a and b show a scatter plot of model simulations of hourly mean g_{sto} values plotted against observed values for the 2015 and 2016 background and peak O_3 treatments for Mulika and Skyfall wheat varieties. All g_{sto} models performed similarly under the background O_3 treatments with R^2 values of between 0.33 and 0.43 and RMSE values between 111 and 137 mmol O_3 m^{-2} s^{-1} with the $A_{net}g_{sto}$*mech* model performing the best. All g_{sto} models performed less well under the peak O_3 treatment with the R^2 range between 0.07 and 0.33, with the $A_{net}g_{sto}$*mech* model performing the best; all models have similar RMSE values. For the peak O_3 treatment, the $A_{net}g_{sto}$*mech* model tends to overestimate g_{sto} whilst the other two models tend to underestimate g_{sto} in relation to the 1:1 line. Similar results were found for A_{net} with values simulated reasonably well under background O_3 treatments by both the $A_{net}g_{sto}$*emp* and $A_{net}g_{sto}$*mech* models with R^2 values of between 0.8 and 0.83 (see Fig. S8a). Both the models tend to underestimate maximum values of A_{net} by ~10 μmol CO_2 m^{-2} PLA s^{-1}.

All models were able to simulate the mean diurnal (see Fig. S9) and mean daily maximum (see Fig. 2c) g_{sto} values equally well for the background O_3 treatment. For the peak O_3 treatments, the $A_{net}g_{sto}$*mech* model tended to overestimate mean diurnal g_{sto} by about 50 mmol O_3 m^{-2} PLA s^{-1} whilst the other two models tended to underestimate g_{sto} by the same margin. Similarly, models were able to simulate the mean diurnal (see Fig. S10) and mean daily maximum A_{net} values (see Fig. S8c) equally well for the background O_3 treatment. As for g_{sto}, all models struggled to predict A_{net} under the peak O_3 treatments with a tendency to overestimate A_{net} in relation to the 1:1 line but to underestimate maximum A_{net} values. A_{net} was comparatively better predicted by the $A_{net}g_{sto}$*mech* model with R^2 values of 0.42 compared to 0.31 for $A_{net}g_{sto}$*emp* model.

Fig. 2c shows that the $A_{net}g_{sto}$*mech* model performs better under peak O_3 concentrations over the full length of the flag leaf lifespan, thus simulating the effect of senescence on g_{sto} reasonably well. By contrast the g_{sto}*emp* and $A_{net}g_{sto}$*emp* models simulated an overly sensitive senescence response of g_{sto} to O_3 compared to the observations. Similar to the g_{sto} results, the $A_{net}g_{sto}$ models overestimated the decline in A_{net} at the end of the growing season compared to the observations (see Fig. S8b). However, the $A_{net}g_{sto}$*mech* model gave a closer fit to the observations than the $A_{net}g_{sto}$*emp* model. It is also worth noting that the $A_{net}g_{sto}$*mech* model simulates higher g_{sto} and A_{net} under the peak O_3 treatment than the low O_3 treatment for the UK. This is because the O_3 effect is most strongly determined by its longer-term impact on senescence than its instantaneous impact on photosynthesis, the former only taking effect once O_3 has brought forward the SOS which occurs only towards the end of the growing season where there are far fewer observed data for comparison.

3.2. Leaf senescence

The CCI data available from the UK (*cv* Mulika) and Swedish (*cv* Dragon) filtration/fumigation datasets were used with the break point method to estimate the SOS and EOS. Results in Fig. 3 show that the higher O_3 treatment (low background *vs* very high peaks for the UK data) brought forwards the SOS by 7 days and EOS by 12 days. Similar results are found for Sweden by comparing the CF *vs* NF++ experiment with SOS and EOS being brought forwards by 6 days and 12 days respectively (see Fig. S11).

The data provided in Table 2 can be used to assess the ability of the $A_{net}g_{sto}$ models to simulate senescence under the different datasets and O_3 treatments used in this study. Table 2 summaries information for the extreme O_3 treatments (i.e. comparing lowest with highest). The difference in O_3 treatment causing senescence effects is indicated by the POD_6 values for the flag leaf lifespan. Table 2 shows that the $A_{net}g_{sto}$*emp* model predicts SOS to occur earlier with a range of 20 days difference compared to the observations, and EOS to generally occur later with a range of 18 days difference compared to the observations. By comparison the $A_{net}g_{sto}$*mech* model simulates SOS closer to the actual date with a range of 8 days earlier to 3 days later and EOS with a range of 8 days earlier to 3 days later compared to the observations. The POD_6 values for the high O_3 treatments are consistently higher for the $A_{net}g_{sto}$*mech* model suggesting that the model is paramterised to be less sensitive to cumulative stomatal O_3 uptake than the $A_{net}g_{sto}$*emp* model. Overall, the mechanistic approach used by the $A_{net}g_{sto}$*mech* model simulated SOS and EOS more closely to the observations. However, care should be made in interpreting these results since the CCI data used to define the actual SOS and EOS are limited in number, leading to some uncertainty in the actual timings of senescence, especially close to anthesis. It should also be noted that the $A_{net}g_{sto}$ models are calibrated against all the CCI data held in the datasets and so there will be some discrepancy when comparing simulations against individual datasets and O_3 treatments.

3.3. Flux-response relationships

Each of the three g_{sto} models were used to develop flux-response relationships based on POD_6 using the O_3 filtration/fumigation data (Fig. 4). The robustness of the flux-response relationship can be determined by the strength of the linear regression (i.e., R^2 value). The $A_{net}g_{sto}$*mech* model ($R^2 = 0.74$) performed better than the g_{sto}*emp* model ($R^2 = 0.68$) in deriving flux-response relationships. The $A_{net}g_{sto}$*emp* model performed slightly less well ($R^2 = 0.66$). The slope of the relationships differ by −0.0412, −0.0342 and −0.0325 for g_{sto}*emp*, $A_{net}g_{sto}$*emp* and $A_{net}g_{sto}$*mech* respectively. This is because the $A_{net}g_{sto}$*mech* model simulates higher g_{sto} values under elevated O_3 and during senescence which will increase the POD_y values. This demonstrates the importance of consistency in using the same g_{sto} method to estimate POD_y as is used to derive the flux-response relationship for yield loss estimates. Were 'critical levels' to be derived from these relationships using the methods described in the LRTAP Convention (2017) (i.e. a 5% reduction in grain yield based on the slope of the relationship) values of 1.69, 1.19 and 1.75 mmol O_3 m^{-2} would be found for g_{sto}*emp*, $A_{net}g_{sto}$*emp* and $A_{net}g_{sto}$*mech* models respectively (also shown as dotted lines in the respective plots in Fig. 4). The range of these values reflects the high g_{sto} values modelled using the $A_{net}g_{sto}$*mech* model. It is useful to note that the dose-response relationships developed in this study are an improvement to those presented in the LRTAP Convention (2017) Mapping Manual (albeit with slightly different data compliments). For comparison, we also show the dose-response relationships developed by applying these three models but only with those datasets used in the LRTAP Convention (2017) Mapping Manual (see Fig. S12).

4. Discussion

We found that the process-based $A_{net}g_{sto}$*mech* model can derive robust flux-based dose-response relationships (with an R^2 value of 0.74), this performance is marginally improved to that of empirical-based

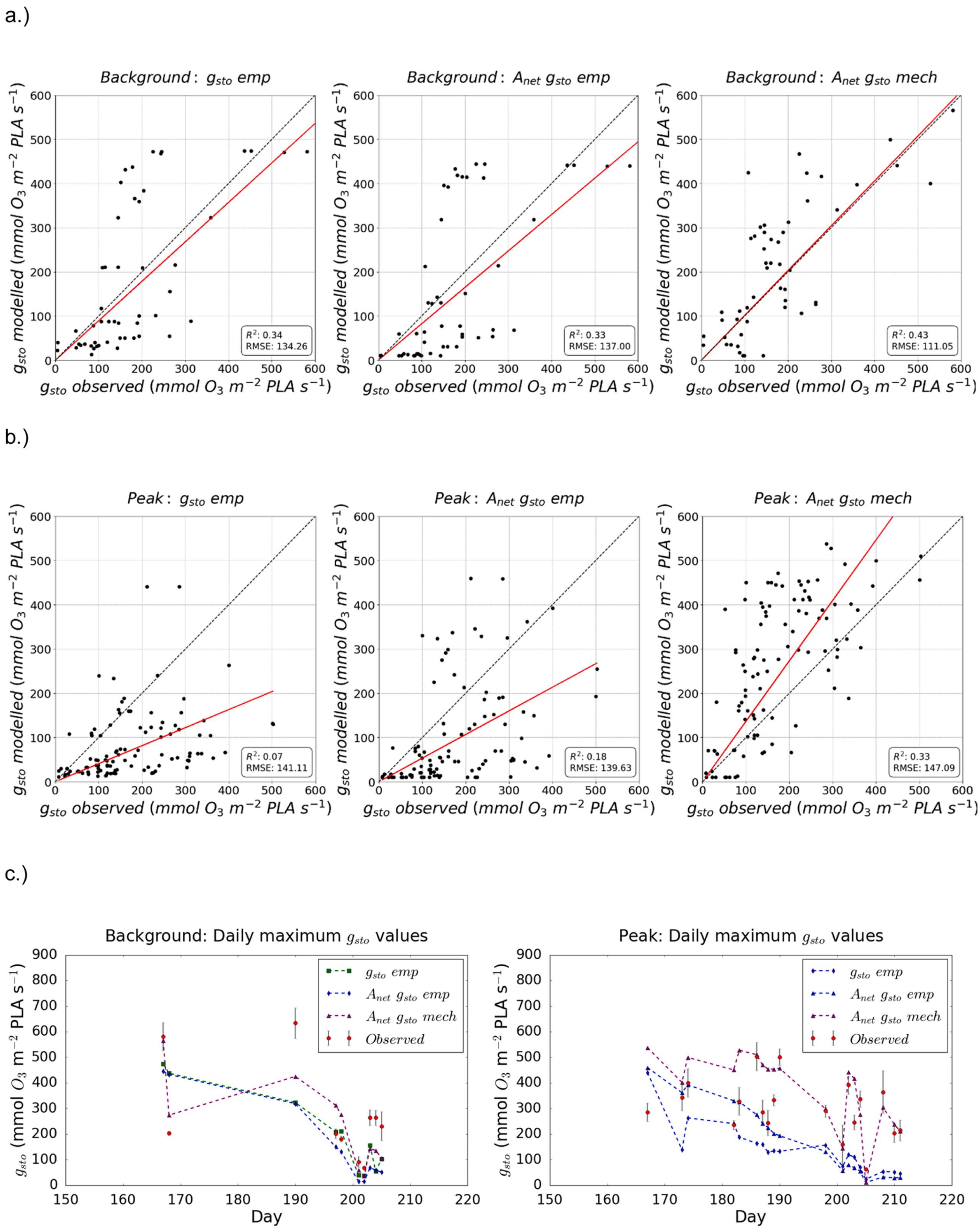

Fig. 2. Plots for background and peak O_3 treatments for Mulika and Skyfall wheat cultivars, fumigated in Bangor over the 2015 and 2016 growing seasons showing a) Observed against modelled g_{sto} values estimated using the three different g_{sto} models. In each plot, the red solid line represents the regression line, showing the relationship between the modelled and observed values. The black dashed line represents the 1:1 line, the coefficient of determination (R^2) and root mean square error (RMSE) is provided for the regression; and b) Average daily maximum g_{sto} values simulated over the flag leaf lifespan by each of the three g_{sto} models and observed daily maximum g_{sto} data. Standard error bars for the observed data are given by black lines extending from the red observed points, providing a visual representation of uncertainty in the measurements.

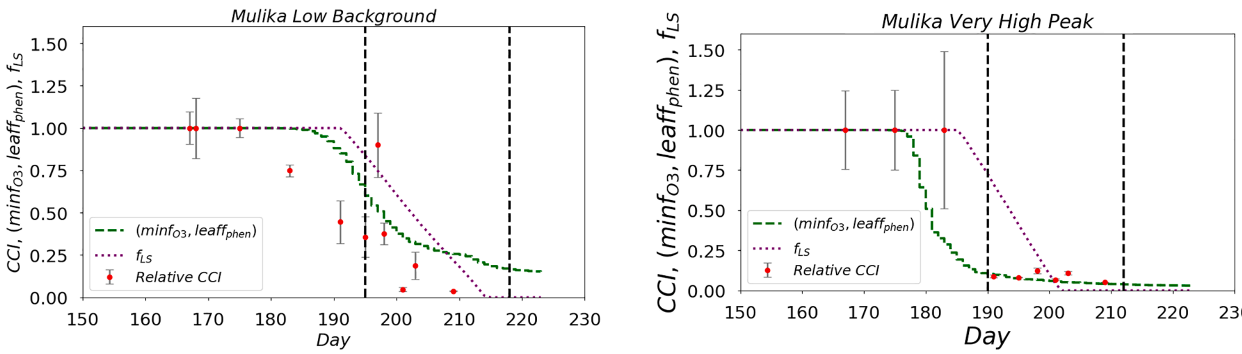

Fig. 3. Leaf senescence profiles of O_3 induced leaf senescence for the Mulika wheat cultivar for the low background (LB) and very high peak (VHP) O_3 treatments in the UK dataset. The timing of the SOS and EOS (vertical dotted black lines) determined by applying the break point method to the CCI data (red circle with standard error bars) are shown in relation to estimates made by the $A_{net}g_{sto}emp$ model (which uses *leaf* f_{phen} and f_{O3} functions to simulate senescence and the $A_{net}g_{sto}mech$ model (which uses f_{LS}) to simulate senescence.

Table 2
Comparison of the difference in days between Start (SOS) and End (EOS) of senescence by site, year and O_3 treatment (described by average 24-hour mean O_3 concentrations in ppb). The "SOS bias" and "EOS bias" columns indicate the deviation in days at SOS and EOS, respectively, from applying the $A_{net}g_{sto}$ models as compared to the observed data. Positive values denote a delay, while negative values signify an advancement in the modelled timing of senescence relative to the observations. Also shown are the POD_y values at SOS and EOS.

Location and Country	Year	Treatments comparison (24-h Mean in ppb)	$A_{net}g_{sto}emp$ SOS bias (in days)	$A_{net}g_{sto}emp$ EOS bias (in days)	$A_{net}g_{sto}emp$ PODy at SOS (mmol m^{-2})	$A_{net}g_{sto}emp$ PODy at EOS (mmol m^{-2})	$A_{net}g_{sto}mech$ SOS bias (in days)	$A_{net}g_{sto}mech$ EOS bias (in days)	$A_{net}g_{sto}mech$ PODy at SOS (mmol m^{-2})	$A_{net}g_{sto}mech$ PODy at EOS (mmol m^{-2})
Ostad, Sweden	1997	CF (11.5)	−6	7	0	0	−8	0	0.13	0.13
		NF+++ (22.2)	−9	1	3.3	6.26	3	−4	5.6	7.94
Ostad, Sweden	1999	CF (17.1)	−9	3	0	0	−6	3	0	0.01
		NF+ (35.2)	−14	−4	4.3	7.5	3	−8	6.9	9.2
Bangor, UK	2015	LB (26.94)	−12	6	2.07	3.3	−4	−1	3.1	4.07
		VHP (55.73)	−9	14	2.78	8.07	1	−4	8.5	11.4

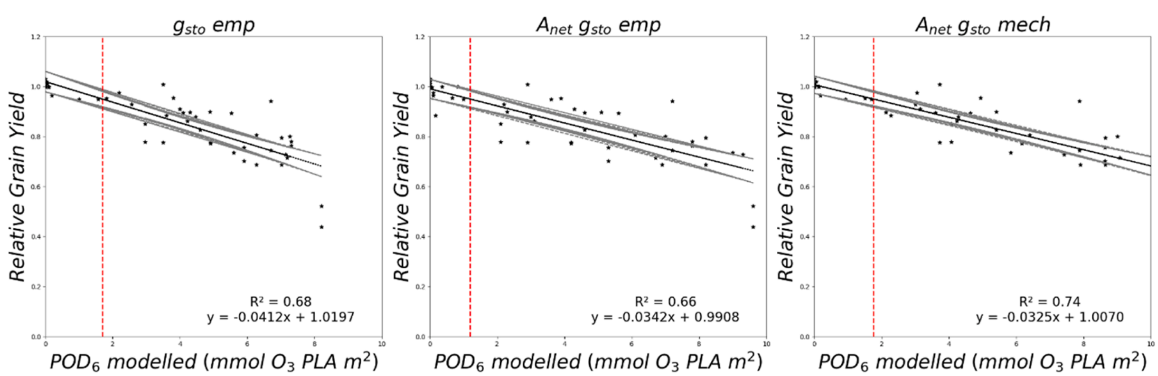

Fig. 4. Flux-response relationships for relative wheat grain yield derived using the three g_{sto} models to simulate the POD_6 metric. The plots replicate the LRTAP Convention (2017) dose-response relationships with the exception of exclusion of an Italian for *Durum* wheat, and inclusion of UK and an additional Swedish dataset. The 95% confidence intervals are indicated by the dotted lines around the best-fit line. The vertical dashed line indicates the 'critical levels' determined by each model. Each figure includes the coefficient of determination (R^2 value) and a dose-response relationship equation.

models ($g_{sto}emp$ and $A_{net}g_{sto}emp$). However, there was little difference (ranging from 1.69 to 1.75 mmol O_3 m^{-2}) in the 'critical levels' derived using each method. This suggests $A_{net}g_{sto}$ models can be reliably used in the derivation of dose-response relationships and 'critical levels' for regional scale risk assessments and that the slope of the dose-response relationship was robust from the point of view of the method to model POD_6. However, even though the variability in slope and 'critical level' values are relatively small, these differences highlight the importance of consistency in application, i.e. that the same g_{sto} algorithm be used to derive the flux (POD_y)-response relationship used in the risk assessment. Our study also found that the $A_{net}g_{sto}mech$ model was better able to simulate the diurnal and seasonal variation in observations of both A_{net} and g_{sto} found under low *vs* high O_3 treatments in the Bangor experiment. This model attribute is particularly advantageous in estimating POD_y given that O_3 concentration profiles can vary substantially across the global wheat growing regions, with some experiencing more chronic O_3 concentrations (e.g., in Europe (Karlsson et al., 2017) while others will experience more extreme, episodic concentrations (e.g., in Asia (Lei, Wuebbles and Liang, 2012)). The results suggest that the $A_{net}g_{sto}mech$ is better able to simulate stomatal O_3 uptake under conditions of higher O_3 concentration. Since the slope of the resulting dose-response relationship does not change, this suggests that the sensitivity of wheat to O_3 uptake remains consistent but that the model is better able to simulate what actual uptake occurs. This finding would warrant further investigation as new datasets become available.

There are three important aspects to accurate A_{net} and g_{sto} estimates, firstly the parameterisation of the leaf level A_{net} model which is dependent upon V_{cmax25}, J_{max25}, m and VPD_0. Secondly, the instantaneous effect of O_3 on A_{net} in relation to its parametrisation and effectiveness in causing O_3 damage. Thirdly, the parameterisation of the module describing O_3 induced leaf senescence, the latter is especially important to estimate A_{net} and g_{sto} toward the end of the growing season, in wheat this coincides with the grain-filling period and is therefore important in determining yield (Neghliz et al., 2016).

Parametrised values for V_{cmax25} and J_{max25} of 88 and 173 μmol CO_2 m^{-2} s^{-1} respectively in this study compare reasonably well to the values of 62–75 and 150–195 μmol CO_2 m^{-2} s^{-1} used for LINTULLC2 (Feng et al., 2022) and AFRCWHEAT (Van Oijen and Ewert, 1999) crop models which incorporate O_3 damage modules for similar European wheat applications. We found limited evidence for variation in V_{cmax25} and J_{max25} with biogeographical region with V_{cmax25} varying between 55 and 180, 53 and 185 and 90 and 120 μmols CO_2 m^{-2} s^{-1} for Atlantic, continental and Mediterranean biogeographic regions respectively; no statistical difference by region was found. This contrasts with the g_{max} value of the g_{sto}*emp* model that has lower values for Mediterranean wheat cultivars (by 70 mmol O_3 m^{-2} s^{-1}, LRTAP Convention (2017)). This study only used experimental data from Atlantic, Boreal or Continental regions. Were Mediterranean data to have been included, the V_{cmax25} and J_{max25} values may have warranted further investigation to establish whether a different $Vc_{\max25}$ might be justified, especially since only 11 datapoints were retrieved for this region in our literature search (see Fig. S3). An indication of this can be provided through comparison with the modelling study presented by Nguyen et al. (2024)Nguyen et al. (2024) which used three crop models (including DO_3SE-Crop, an extension of the $A_{net}g_{sto}$ type of model described here to estimate carbon allocation, growth, and yield). Here the DO_3SE-Crop model was parameterised for a Mediterranean variety of spring wheat (*Califa sur*) with values of key photosynthetic model parameters being 102 μmol CO_2 m^{-2} s^{-1} for V_{cmax25}, 194 μmol CO_2 m^{-2} s^{-1} for J_{max25}, 8.57 for m and 2.2 kPa for D_0. These Mediterranean values for V_{cmax25} and J_{max25} are both somewhat lower (by ~ 14 and 20 μmol CO_2 m^{-2} s^{-1} respectively) than those used in this study and hence would suggest that the $A_{net}g_{sto}$ model would benefit from a Mediterranean parameterisation similar to the regional parameterisations used in the g_{sto}*emp* model.

One other important consideration in relation to geographical region is the effect of soil moisture on g_{sto} since the Mediterranean region is likely to experience longer and more extreme periods of drought stress that will reduce stomatal O_3 uptake (Fagnano et al., 2009). This is particularly important for wheat since this tends to be a rainfed crop in Europe. A variety of methods have been developed to simulate the effect of soil water status (described variously as soil water potential (referred to in this study as f_{swp}), soil water content or plant available water (Büker et al., 2007) on g_{sto}. These methods can be used in either the g_{sto}*emp* or $A_{net}g_{sto}$*emp* type models (the latter by including the f_{swp} function as a multiplier in the A_c formulation (see Eq. (3)). We were unable to test the effectiveness of this aspect of the modelling since the datasets used in this analysis all represented well-watered conditions. However, this would be an important aspect to investigate further, especially in relation to model application, to ensure g_{sto}*emp* and $A_{net}g_{sto}$*emp* models respond similarly (in terms of magnitude of changes to stomatal O_3 flux) to the inclusion of these soil water status parameters.

The ratio between V_{cmax25} and J_{max25} was found to vary between 0.2 and 0.8 (Fig. S3) and was calibrated to a value of 0.51 for this dataset. This is consistent with a study by Wullschleger (1993) who found a ratio of 0.38–0.55 for wheat even as growth and temperature varied. However, other research found that the ratio may range from 1 to 3 (Camino et al., 2019; Day,Station and Al, 1982) which may be attributed to J_{max25} being more reliant on light than V_{cmax25} causing the ratio to decrease when light intensity decreases (Dai et al., 2004). The value of 7.87 for m used in this study is also within the range of 5 and 15 found for many different cultivars of wheat (Kosugi et al., 2003; Collatz et al., 1991; Baldocchi and Meyers, 1998; Miner,Bauerle and Baldocchi, 2017). The VPD_0 value is markedly different (2.2 kPa) from that of Luening et al. (1995) and means that A_{net} can be maintained under high values of VPD, this is consistent with the f_{VPD} relationship and observational data (Danielsson et al., 2003).

The validity of the $A_{net}g_{sto}$*mech* model also depends on appropriate formulation and parameterisation of the key O_3 damage mechanisms. These damage mechanisms are assumed to have both an instantaneous ($f_{O3,s}(d)$) effect of O_3 on photosynthesis and a longer-term effect (f_{LS}) of accumulated O_3 uptake promoting earlier senescence. The instantaneous effect reduces carboxylation *via* a reduction in rubisco activity which may in turn lead to a reduction in carbon assimilation when Rubisco activity (A_c) is limiting net photosynthesis. This reduction in Rrubisco activity is assumed to repair overnight but with repair effectiveness decreasing as the leaf ages. According to Farage et al. (1991), the instantaneous impact of O_3 was only seen with a significant reduction in carboxylation efficiency (>50 %) causing a reduction in carbon assimilation. This could happen when crops are exposed to elevated O_3 concentrations for long periods or if repeated high O_3 exposures were to take place causing the crop to lose its ability to recover (Feng et al., 2022). By contrast, the length of the leaf senescence period is essential for determining the crop development cycle (Ding et al., 2023). The onset of leaf senescence causes a substantial decrease in carbon assimilation (A_{net}), primarily attributed to changes in chloroplast structure and function, and hence the chlorophyll content in the flag leaf (Ding et al., 2023; Gelang et al., 2000; Ojanperä et al.,1998), and contributes to the reduction in dry ear weight, which directly affects yield loss (Gelang et al., 2000). The CCI has been shown to be a good predictor of the onset of senescence (Mariën et al., 2019; Osborne et al., 2019). It can also be used as a proxy for V_{cmax25} (Croft et al., 2017), which is our modelling approach since we assume SOS will coincide with a reduction in V_{cmax25} and consequently A_c (see Eq. (8)). We find that the $A_{net}g_{sto}$*mech* model can simulate SOS and EOS for the elevated O_3 treatments in the UK and Sweden data better than the empirical models. For the UK, the flag leaf starts to senesce 6 days earlier in high (VHP) compared to low (LB) O_3 treatment, for Sweden 7 days earlier in high (NF+++) compared to carbon-filtered (CF) treatments. The number of days by which high O_3 levels can bring forward the start of senescence is corroborated by other published studies (Pleijel et al., 1997; Grandjean and Fuhrer, 1989; Gelang et al., 2000) which found the flag leaf could senesce up to 25 days earlier in the very high O_3 compared to the carbon filtered treatments. O_3 was also found to cause differences in the maturity (EOS)of the flag leaf; Shi et al. (2009) reported that maturity (EOS) occured 8 days earlier in elevated O_3 (50 % higher than ambient) compared to ambient O_3 treatments. Similar results were found in this study, with the flag leaf modelled to reach maturity (EOS)12 days earlier in VHP compared to LB treatments. Although our results seem consistent, they are based on a limited number of CCI data points (11 and 13 for each treatment for the UK and Sweden respectively) which are only captured from mid-anthesis to 10 days before maturity. Additional CCI data spread more evenly over the crucial crop growth period would improve our understanding of how O_3 affects senescence.

Parameters for the $A_{net}g_{sto}$ models were found using an automated calibration method, the genetic algorithm optimisation technique since this approach is considered superior in performance to more traditional techniques (Kuo et al., 2000; Dai et al., 2009; Vazquez-Cruz et al., 2014). The genetic algorithm method was also chosen since it works with a range of parameter searches from a population of points and employs probabilistic transition rules, i.e., uses random sets of parameters instead of using fixed sets, which makes the optimisation process more robust (Kuo,Merkley and Liu, 2000). This study demonstrated the effectiveness of this approach with the five training samples that are used to form dose-response relationships giving RMSE ranges from 0.99 to 4.5 × 10^{-5} mmol m^{-2} for the $A_{net}g_{sto}$*mech* model (data not shown).

Such a good performance suggests that the parametrisation derived can give robust values for the $A_{net}g_{sto}$ models for use in other European O_3 risk assessment applications.

The calibration approach to parameterise the $A_{net}g_{sto}$ models is different to that used to parameterise the $g_{sto}emp$ model which identifies g_{max} and f_{min} values (as average maximum and minimum values respectively) and the f functions using a boundary line analysis method (LRTAP Convention, 2017). Since the A_{net} models are effectively calibrated to the output of a sub-set of all datasets it can be argued that this may improve the ability of this model type compared to the $g_{sto}emp$ model. It is also important to note that the A_{net} models calibration included the UK Bangor dataset (and hence additional information on the onset and rate of senescence) as compared to the parameterisation of the $g_{sto}emp$ model, these data would have been useful to test and inform the existing $g_{sto}emp\ f_{O3}$ function. Ideally, all models would be calibrated using the same data and methods, which would mean that the $g_{sto}emp$ model would be calibrated using the genetic algorithm method and with the inclusion of the UK data describing senescence. Although such work was outside the scope of the current study it would be useful to consider in future modelling studies. As such unequivocal claims that $A_{net}g_{sto}$ models are better than $g_{sto}emp$ models need to be made with caution.

5. Conclusion

Overall, we find that the $A_{net}g_{sto}mech$ model can be used to derive robust flux-response relationships when incorporating both short- and long-term O_3 damage processes. The $A_{net}g_{sto}mech$ model also has the added benefit of achieving reasonable estimates of g_{sto} under variable O_3 concentrations and has a direct link to carbon assimilation. This study's establishment of an $A_{net}g_{sto}mech$ flux-response relationship could be used to calibrate or constrain models that use the $A_{net}g_{sto}$ approach (e.g. photosynthesis based crop models, land surface exchange models, biogeochemical cycling models and earth system models) thus supporting a move towards more process-based assessments of O_3 damage and yield loss.

CRediT authorship contribution statement

P. Pande: Conceptualization, Methodology, Validation, Writing – original draft, Writing – review & editing. **F. Hayes:** Conceptualization, Data curation. **S. Bland:** Software. **N. Booth:** Conceptualization. **H. Pleijel:** Conceptualization, Data curation. **L.D. Emberson:** Conceptualization, Supervision, Writing – review & editing.

Declaration of competing interest

The authors declare that they have no known competing financial interests or personal relationships that could have appeared to influence the work reported in this paper.

Data availability

Data will be made available on request.

Acknowledgements

This research did not receive any specific grant from funding agencies in the public, commercial, or not-for-profit sectors.

Supplementary materials

Supplementary material associated with this article can be found, in the online version, at doi:10.1016/j.agrformet.2024.110150.

References

Anav, A., De Marco, A., Proietti, C., Alessandri, A., Dell'Aquila, A., Cionni, I., Friedlingstein, P., Khvorostyanov, D., Menut, L., Paoletti, E., et al., 2016. Comparing concentration-based (AOT40) and stomatal uptake (PODY) metrics for ozone risk assessment to European forests. Glob. Change Biol. 22 (4), 1608–1627. https://doi.org/10.1111/gcb.13138 [Online]. Available at[Accessed 28 February 2021].

Arnold, S., Kanter, D., Lombardozzi, D., Tai, A.P.K., Sadiq, M., Pang, J.Y.S., Yung, D.H.Y., Feng, Z., 2021. Impacts of surface ozone pollution on global crop yields: comparing different ozone exposure metrics and incorporating Co-effects of CO 2. Front impacts of surface ozone pollution on global crop yields: comparing different ozone exposure metrics and incor. Sustain. Food Syst. 5, 534616 https://doi.org/10.3389/fsufs.2021.534616 [Online]. Available at.

Baldocchi, D., Meyers, T., 1998. On using eco-physiological, micrometeorological and biogeochemical theory to evaluate carbon dioxide, water vapor and trace gas fluxes over vegetation: a perspective. Agric. For. Meteorol. 90 (1–2), 1–25. https://doi.org/10.1016/S0168-1923(97)00072-5 [Online]. Available at:

Ball, J.T., Woodrow, I.E., Berry, J.A., 1987. Progress in Photosynthesis Research. Progress in Photosynthesis Research. https://doi.org/10.1007/978-94-017-0519-6 (January 2015). [Online]. Available at:

Betzelberger, A.M., Yendrek, C.R., Sun, J., Leisner, C.P., Nelson, R.L., Ort, D.R., Ainsworth, E.A., 2012. Ozone exposure response for U.S. soybean cultivars: linear reductions in photosynthetic potential, biomass, and yield. Plant Physiol. 160 (4), 1827–1839. https://doi.org/10.1104/pp.112.205591 [Online]. Available at.

S. Boleti, E., Hueglin, C., Grange, K., Takahama, S., 2020. Temporal and spatial analysis of ozone concentrations in Europe based on timescale decomposition and a multi-clustering approach Atmos. Chem. Phys. 20 (14), 9051–9066. https://doi.org/10.5194/acp-20-9051-2020 [Online]. Available at.

Büker, P., Emberson, L.D., Ashmore, M.R., Cambridge, H.M., Jacobs, C.M.J., Massman, W.J., Müller, J., Nikolov, N., Novak, K., Oksanen, E., et al., 2007. Comparison of different stomatal conductance algorithms for ozone flux modelling. Environ. Pollut. 146 (3), 726–735. https://doi.org/10.1016/j.envpol.2006.04.007 [Online]. Available at.

Büker, P., Feng, Z., Uddling, J., Briolat, A., Alonso, R., Braun, S., Elvira, S., Gerosa, G., Karlsson, P.E., Le Thiec, D., et al., 2015. New flux based dose-response relationships for ozone for European forest tree species. Environ. Pollut. 206, 163–174. https://doi.org/10.1016/j.envpol.2015.06.033 [Online]. Available at[Accessed 30 January 2021].

Camino, C., Gonzalez-dugo, V., Hernandez, P., Zarco-tejada, P.J., 2019. Remote sensing of environment radiative transfer Vcmax estimation from hyperspectral imagery and SIF retrievals to assess photosynthetic performance in rainfed and irrigated plant phenotyping trials. Remote Sens. Environ. 231, 111186 https://doi.org/10.1016/j.rse.2019.05.005 (May)[Online]. Available at:

Collatz, G.J., Ball, J.T., Grivet, C., Berry, J.A., 1991. Physiological and environmental regulation of stomatal conductance, photosynthesis and transpiration: a model that includes a laminar boundary layer. Agric. For. Meteorol. 54 (2–4), 107–136. https://doi.org/10.1016/0168-1923(91)90002-8 [Online]. Available at:

Croft, H., Chen, J.M., Luo, X., Bartlett, P., Chen, B., Staebler, R.M., 2017. Leaf chlorophyll content as a proxy for leaf photosynthetic capacity. Glob. Change Biol. 23 (9), 3513–3524. https://doi.org/10.1111/gcb.13599 [Online]. Available at:

Dai, C., Yao, M., Xie, Z., Chen, C., Liu, J., 2009. Parameter optimization for growth model of greenhouse crop using genetic algorithms. Appl. Soft Comput. J. 9 (1), 13–19. https://doi.org/10.1016/J.ASOC.2008.02.002 [Online]. Available at:

Dai, Y., Dickinson, R.E., Wang, Y.P., 2004. A two-big-leaf model for canopy temperature, photosynthesis, and stomatal conductance. J. Clim. 17 (12), 2281–2299. https://doi.org/10.1175/1520-0442(2004)017<2281:ATMFCT>2.0.CO;2 [Online]. Available at:

Danielsson, H., Karlsson, G.P., Karlsson, P.E., Pleijel, H., 2003. Ozone uptake modelling and flux-response relationships - an assessment of ozone-induced yield loss in spring wheat. Atmos. Environ. 37 (4), 475–485. https://doi.org/10.1016/S1352-2310(02)00924-X. Pergamon[Online]. Available at:

Day, W., Station, R.E. and Al, H. (1982). Application to wheat and barley of two leaf photosynthesis models for C 3 plants. 5, pp.501–507.

Ding, Y., Zhang, X., Ma, Q., Li, F., Tao, R., Zhu, M., Li, C., Zhu, X., Guo, W., Ding, J., 2023. Tiller fertility is critical for improving grain yield, photosynthesis and nitrogen efficiency in wheat. J. Integr. Agric. 22 (7), 2054–2066. https://doi.org/10.1016/j.jia.2022.10.005 [Online]. Available at:

Emberson, L.D., Ashmore, M.R., Cambridge, H.M., Simpson, D., Tuovinen, J.P., 2000. Modelling stomatal ozone flux across Europe. Environ. Pollut. 109 (3), 403–413. https://doi.org/10.1016/S0269-7491(00)00043-9 [Online]. Available at:

Emberson, L.D., Pleijel, H., Ainsworth, E.A., van den Berg, M., Ren, W., Osborne, S., Mills, G., Pandey, D., Dentener, F., Büker, P., et al., 2018. Ozone effects on crops and consideration in crop models. Eur. J. Agron. 100 (May), 19–34. https://doi.org/10.1016/j.eja.2018.06.002 [Online]. Available at:

Ewert, F., Porter, J.R., 2000. Ozone effects on wheat in relation to CO2: modelling short-term and long-term responses of leaf photosynthesis and leaf duration. Glob. Change Biol. 6 (7), 735–750. https://doi.org/10.1046/j.1365-2486.2000.00351.x [Online]. Available at:

Farage, P.K., Long, S.P., Lechner, E.G., Baker, N.R., 1991. The sequence of change within the photosynthetic apparatus of wheat following short-term exposure to ozone. Plant Physiol. 95 (2), 529–535. https://doi.org/10.1104/pp.95.2.529 [Online]. Available at:

Farquhar, G.D., von Caemmerer, S., Berry, J.A., 1980. A biochemical model of photosynthetic CO2 assimilation in leaves of C3 species. Planta 149, 78–90.

Fagnano, M., Maggio, A., Fumagalli, I., 2009. Crops' responses to ozone in Mediterranean environments. Environ. Pollut. 157, 1438–1444. https://doi.org/10.1016/j.envpol.2008.09.001.

Feng, Y., Nguyen, T.H., Alam, M.S., Emberson, L., Gaiser, T., Ewert, F., Frei, M., 2022. Identifying and modelling key physiological traits that confer tolerance or sensitivity to ozone in winter wheat. Environ. Pollut. 304 (April), 119251 https://doi.org/10.1016/j.envpol.2022.119251 [Online]. Available at:

Feng, Z., Agathokleous, E., Yue, X., Oksanen, E., Paoletti, E., Sase, H., Gandin, A., Koike, T., Calatayud, V., Yuan, X., et al. (2021). *Emerging challenges of ozone impacts on asian plants: actions are needed to protect ecosystem health.* [Online]. Available at: doi:10.1080/20964129.2021.1911602 [Accessed 6 June 2022].

Feng, Z., Kobayashi, K., Li, P., Xu, Y., Tang, H., Guo, A., Paoletti, E., Calatayud, V., 2019. Impacts of current ozone pollution on wheat yield in China as estimated with observed ozone, meteorology and day of flowering. Atmos. Environ. 217, 116945 https://doi.org/10.1016/j.atmosenv.2019.116945. September[Online]. Available at:

Gelang, J., Pleijel, H., Sild, E., Danielsson, H., Younis, S., Selldén, G., 2000. Rate and duration of grain filling in relation to flag leaf senescence and grain yield in spring wheat (Triticum aestivum) exposed to different concentrations of ozone. Physiologia Plantarum 110 (3), 366–375. https://doi.org/10.1111/J.1399-3054.2000.1100311.X [Online]. Available at:

Ghosh, A., Agrawal, M., Agrawal, S.B., 2020. Effect of water deficit stress on an Indian wheat cultivar (Triticum aestivum L. HD 2967) under ambient and elevated level of ozone. Sci. Total Environ. 714, 136837 https://doi.org/10.1016/j.scitotenv.2020.136837 [Online]. Available at:

Grandjean, A. and Fuhrer Grandjean, J. (1989). Growth and leaf senescence in spring wheat (Triticum aestivum) grown at different ozone concentrations in open-top field chambers. 77.

Grote, U., Fasse, A., Nguyen, T.T., Erenstein, O., 2021. Food security and the dynamics of wheat and maize value chains in Africa and Asia. Frontiers in Sustainable Food Systems. 4, Frontiers Media S.A, 617009. https://doi.org/10.3389/fsufs.2020.617009 [Online]. Available at:[Accessed 31 May 2021].

Grulke, N.E. and Heath, & RL (2019). Ozone effects on plants in natural ecosystems. [Online]. Available at: doi:10.1111/plb.12971.

Grünhage, L., Pleijel, H., Mills, G., Bender, J., Danielsson, H., Lehmann, Y., Castell, J.F., Bethenod, O., 2012. Updated stomatal flux and flux-effect models for wheat for quantifying effects of ozone on grain yield, grain mass and protein yield. Environ. Pollut. 165, 147–157. https://doi.org/10.1016/J.ENVPOL.2012.02.026 [Online]. Available at:

Hansen, E.M.Ø., Hauggaard-Nielsen, H., Launay, M., Rose, P., Mikkelsen, T.N., 2019. The impact of ozone exposure, temperature and CO2 on the growth and yield of three spring wheat varieties. Environ. Exp. Bot. 168. https://doi.org/10.1016/J.ENVEXPBOT.2019.103868 [Online]. Available at:

Harley, P.C., Thomas, R.B., Reynolds, J.F., Strain, B.R., 1992. Modelling photosynthesis of cotton grown in elevated CO2. Plant, Cell Environ. 15 (3), 271–282. https://doi.org/10.1111/j.1365-3040.1992.tb00974.x [Online]. Available at:

Hesterberg, T., 2011. Bootstrap. 3, John Wiley & Sons, Inc. WIREs Comp Stat, pp. 497–526. https://doi.org/10.1002/wics.182 [Online]. Available at:

Jarvis, P.G., 1976. The interpretation of the variations in leaf water potential and stomatal conductance found in canopies in the field. Phil. Trans. R. Soc. Lond. Ser. B 273, 593–610.

Karlsson, P.E., Klingberg, J., Engardt, M., Andersson, C., Langner, J., Karlsson, G.P., Pleijel, H., 2017. Past, present and future concentrations of ground-level ozone and potential impacts on ecosystems and human health in northern Europe. Sci. Total Environ. 576, 22–35. https://doi.org/10.1016/J.SCITOTENV.2016.10.061 [Online]. Available at:

Kosugi, Y., Shibata, S., Kobashi, S. and Caemmerer, V. (2003). Parameterization of the CO2 and H2O gas exchange of several temperate deciduous broad-leaved trees at the leaf. pp.285–301.

Kuo, S.F., Merkley, G.P., Liu, C.W., 2000. Decision support for irrigation project planning using a genetic algorithm. Agric. Water Manag. 45 (3), 243–266. https://doi.org/10.1016/S0378-3774(00)00081-0 [Online]. Available at:

Lei, H., Wuebbles, D.J., Liang, X.Z., 2012. Projected risk of high ozone episodes in 2050. Atmos. Environ. 59, 567–577. https://doi.org/10.1016/J.ATMOSENV.2012.05.051 [Online]. Available at:

Leuning, R., 1995. A critical appraisal of combine stomatal model C3 plants. Plant, Cell Environ. 18, 339–355 [Online]. Available at: http://www.unc.edu/courses/2010spring/geog/595/001/www/Leuning95b-PCE.pdf%0Apapers2://publication/uuid/B8B998AB-EB42-4E09-A609-B192084D13EE.

Leuning, R., Dunin, F.X. and Wang, Y. (1998). A two-leaf model for canopy conductance, photosynthesis and partitioning of available energy . II . Comparison with measurements. 91, pp.113–125.

Liu, X., Sun, H., Feike, T., Zhang, X., Shao, L. and Chen, S. (2016). Assessing the impact of air pollution on grain yield of winter wheat - a case study in the North China Plain. Hui, D. (Ed). *PLOS ONE*, 11 (9), Public Library of Science., p. e0162655. [Online]. Available at: doi:10.1371/journal.pone.0162655 [Accessed 18 September 2020].

LRTAP Convention, 2017. Manual on methodologies and criteria for modelling and mapping critical loads and levels and air pollution effects, risks and trends. Chapter 3 Mapp. Crit. levels Veg. 66. http://icpvegetation.ac.uk. Accessed date: 16 May 2017.

Mariën, B., Balzarolo, M., Dox, I., Leys, S., Lorène, M.J., Geron, C., Portillo-Estrada, M., AbdElgawad, H., Asard, H., Campioli, M., 2019. Detecting the onset of autumn leaf senescence in deciduous forest trees of the temperate zone. New Phytol. 224 (1), 166–176. https://doi.org/10.1111/NPH.15991 [Online]. Available at:[Accessed 11 October 2021].

Massman, W.J., Musselman, R.C., Lefohn, A.S., 2000. A conceptual ozone dose-response model to develop a standard to protect vegetation. Atmos. Environ. 34 (5), 745–759. https://doi.org/10.1016/S1352-2310(99)00395-7. Pergamon.[Online]. Available at:

Medlyn, B.E., Duursma, R.A., Eamus, D., Ellsworth, D.S., Prentice, I.C., Barton, C.V.M., Crous, K.Y., De Angelis, P., Freeman, M., Wingate, L., 2011. Reconciling the optimal and empirical approaches to modelling stomatal conductance. Glob. Change Biol. 17 (6), 2134–2144. https://doi.org/10.1111/j.1365-2486.2010.02375.x [Online]. Available at:

Mills, G., Hayes, F., Simpson, D., Emberson, L., Norris, D., Harmens, H., Büker, P., 2011. Evidence of widespread effects of ozone on crops and (semi-)natural vegetation in Europe (1990–2006) in relation to AOT40- and flux-based risk maps. Glob. Change Biol. 17 (1), 592–613. https://doi.org/10.1111/J.1365-2486.2010.02217.X [Online]. Available at:[Accessed 7 March 2023].

Mills, G., Sharps, K., Simpson, D., Pleijel, H., Frei, M., Burkey, K., Emberson, L., Uddling, J., Broberg, M., Feng, Z., et al., 2018. Closing the global ozone yield gap: quantification and cobenefits for multistress tolerance. Glob. Change Biol. 24 (10), 4869–4893. https://doi.org/10.1111/gcb.14381 [Online]. Available at:

Miner, G.L., Bauerle, W.L., Baldocchi, D.D., 2017. Estimating the sensitivity of stomatal conductance to photosynthesis: a review. Plant, Cell Environ. 40 (7), 1214–1238. https://doi.org/10.1111/pce.12871 [Online]. Available at:[Accessed 8 April 2021].

Neghliz, H., Cochard, H., Brunel, N., Martre, P., 2016. Ear rachis xylem occlusion and associated loss in hydraulic conductance coincide with the end of grain filling for wheat. Front. Plant Sci. 7, 1–11. https://doi.org/10.3389/fpls.2016.00920. June [Online]. Available at:

Van Oijen, M., Ewert, F., 1999. The effects of climatic variation in Europe on the yield response of spring wheat cv. Minaret to elevated CO2 and O3: an analysis of open-top chamber experiments by means of two crop growth simulation models. Eur. J. Agron. 10 (3–4), 249–264. https://doi.org/10.1016/S1161-0301(99)00014-3 [Online]. Available at:

Ojanperä, K., Pätsikkä, E., Yläranta, T., 1998. Effects of low ozone exposure of spring wheat on net CO2 uptake, Rubisco, leaf senescence and grain filling. New Phytol. 138 (3), 451–460. https://doi.org/10.1046/J.1469-8137.1998.00120.X [Online]. Available at:[Accessed 3 February 2022].

Op De Beeck, M., et al., 2010. A comparison of two stomatal conductance models for ozone flux modelling using data from two Brassica species. Environ. Pollut. 158 (10), 3251–3260. https://doi.org/10.1016/j.envpol.2010.07.026.

Osborne, S., Pandey, D., Mills, G., Hayes, F., Harmens, H., Gillies, D., Büker, P., Emberson, L., 2019. New insights into leaf physiological responses to ozone for use in crop Modelling. Plants 8 (4). https://doi.org/10.3390/plants8040084 [Online]. Available at:

Pleijel, H., Danielsson, H., Broberg, M.C., 2022. Benefits of the Phytotoxic Ozone Dose (POD) index in dose-response functions for wheat yield loss. Atmos. Environ. 268, 118797 https://doi.org/10.1016/J.ATMOSENV.2021.118797. Pergamon[Online]. Available at:

Pleijel, H., Danielsson, H., Emberson, L., Ashmore, M.R., Mills, G., 2007. Ozone risk assessment for agricultural crops in Europe: further development of stomatal flux and flux-response relationships for European wheat and potato. Atmos. Environ. 41 (14), 3022–3040. https://doi.org/10.1016/j.atmosenv.2006.12.002 [Online]. Available at:

Pleijel, H., Ojanperä, K., Danielsson, H., Sild, E., Gelang, J., Wallin, G., Skärby, L., Selldén, G., 1997. Effects of ozone on leaf senescence in spring wheat - possible consequences for grain yield. Phyton - Annales Rei Botanicae 37 (3), 227–232.

Rega, C., Short, C., Pérez-Soba, M., Luisa Paracchini, M., 2020. A classification of European agricultural land using an energy-based intensity indicator and detailed crop description. Landsc. Urban Plan. 198 https://doi.org/10.1016/j.landurbplan.2020.103793 (March)[Online]. Available at:

Shah, S.H., Wagner, C.H., Sanga, U., Park, H., Demange, L.H.M., de, L., Gueiros, C., Niles, M.T., 2019. Does household capital mediate the uptake of agricultural land, crop, and livestock adaptations? Evidence from the Indo-Gangetic plains (India). In: Frontiers in Sustainable Food Systems, p. 3. https://doi.org/10.3389/fsufs.2019.00001 (January). [Online]. Available at:

Sharkey, T.D., Bernacchi, C.J., Farquhar, G.D., Singsaas, E.L., 2007. Fitting photosynthetic carbon dioxide response curves for C(3) leaves. Plant, Cell Environ. 30 (9), 1035–1040. https://doi.org/10.1111/j.1365-3040.2007.01710.x [Online]. Available at:

Shi, G., Yang, L., Wang, Y., Kobayashi, K., Zhu, J., Tang, H., Pan, S., Chen, T., Liu, G., Wang, Y., 2009. Impact of elevated ozone concentration on yield of four Chinese rice cultivars under fully open-air field conditions. Agric., Ecosyst. Environ. 131 (3–4), 178–184. https://doi.org/10.1016/J.AGEE.2009.01.009 [Online]. Available at.

Sicard, P., Agathokleous, E., De Marco, A., Paoletti, E., Calatayud, V., 2021. Urban population exposure to air pollution in Europe over the last decades. Environ. Sci. Eur. 33 (1), 1–12. https://doi.org/10.1186/S12302-020-00450-2. *2021 33:1* [Online]. Available at:[Accessed 10 October 2021].

Simpson, D., Benedictow, A., Berge, H., Bergström, R., Emberson, L.D., Fagerli, H., Flechard, C.R., Hayman, G.D., Gauss, M., Jonson, J.E., et al., 2012. The EMEP MSC-W chemical transport model – Technical description. Atmos. Chem. Phys. 12 (16), 7825–7865. https://doi.org/10.5194/ACP-12-7825-2012 [Online]. Available at:

Sharma, D.K., et al., 2015. Wheat cultivars selected for high F v /F m under heat stress maintain high photosynthesis, total chlorophyll, stomatal conductance, transpiration and dry matter. Physiologia Plantarum 153, 284–298. https://doi.org/10.1111/ppl.12245.

Tai, A.P.K., Sadiq, M., Pang, J.Y.S., Yung, D.H.Y., Feng, Z., 2021. Impacts of surface ozone pollution on global crop yields: comparing different ozone exposure metrics and incorporating Co-effects of CO2. Fron. Sustain. Food Syst. 5, 534616 https://doi.org/10.3389/fsufs.2021.534616 [Online]. Available at:[Accessed 31 May 2021].

Uddling, J., Pleijel, H., 2006. Changes in stomatal conductance and net photosynthesis during phenological development in spring wheat: implications for gas exchange modelling. Int. J. Biometeorol. 51 (1), 37–48. https://doi.org/10.1007/s00484-006-0039-6.

Vazquez-Cruz, M.A., Guzman-Cruz, R., Lopez-Cruz, I.L., Cornejo-Perez, O., Torres-Pacheco, I., Guevara-Gonzalez, R.G., 2014. Global sensitivity analysis by means of EFAST and Sobol' methods and calibration of reduced state-variable TOMGRO model using genetic algorithms. Comput. Electr. Agric. 100, 1–12. https://doi.org/10.1016/J.COMPAG.2013.10.006 [Online]. Available at:

Wang, Q.J., 1997. Using genetic algorithms to optimise model parameters. Environ. Model. Softw. 12 (1), 27–34. https://doi.org/10.1016/S1364-8152(96)00030-8 [Online]. Available at:

Wang, S., Yang, Y., Trishchenko, A.P., Barr, A.G., Black, T.A., McCaughey, H., 2009. Modeling the response of canopy stomatal conductance to humidity. J. Hydrometeorol. 10 (2), 521–532. https://doi.org/10.1175/2008JHM1050.1 [Online]. Available at:[Accessed 5 October 2021].

Wullschleger, S.D. (1993). Biochemical limitations to carbon assimilation in C 3 plants — a retrospective analysis of the A /C i curves from 109 species biochemical limitations to carbon assimilation in C3 plants — a retrospective analysis of the A / C ¡ curves from 109 species. 44 (262), pp.907–920.

United States Department of Agriculture (USDA). (2023). World agricultural supply and demand estimates (WASDE).

Nguyen, T.H., Cappelli, G.A., Emberson, L., Fernandez Ignacio, G., Irimescu, A., Francesco, S., Fabrizio, G., Booth, N., Boldeanu, G., Bermejo, V., Bland, S., Frei, M., Ewert, F., Gaiser, T., 2024. Assessing the spatio-temporal tropospheric ozone and drought impacts on leaf growth and grain yield of wheat across Europe through crop modeling and remote sensing data. European Journal of Agronomy 153, 127052.